Modeling the Interaction Between Bristle Elastic Structures and Fluids

N.D. Botkin, K.-H. Hoffmann, V.N. Starovoitov, V.L. Turova

Center of Advanced European Studies and Research (caesar)
Friedensplatz 16, 53111 Bonn, Germany
botkin@caesar.de, hoffmann@caesar.de, starovoitov@caesar.de, turova@caesar.de

ABSTRACT

The interaction of a bristle structure with a fluid is studied. Such a problem arises, for example, when modeling biotechnological devices operating in liquids or when simulating epithelium surfaces of blood vessels. In the paper, a homogenized model of the bristle structure is proposed. The interaction between the bristles and the fluid is replaced by an averaged material whose properties are derived using the passage to the limit in the model based on the fluid-solid interface conditions as the number of the bristles goes to infinity whereas their thickness goes to zero. Based on the model of the averaged material, the computation of sensitivity characteristics for a Love wave sensor is done.

Keywords: Multi-layered structure, Fluid-solid interface, Homogenization, Biosensor.

1 INTRODUCTION

This investigation is motivated by modeling a surface acoustic wave sensor based on the generation and detection of horizontally polarized shear waves (see [1]). Acoustic shear waves are excited due to an alternate voltage applied to electrodes deposited on a quartz crystal substrate. The waves are transmitted into a thin isotropic guiding layer covered by a thin gold film that contacts a liquid containing a ligand to be detected. The ligand adheres to a specific receptor (aptamer) immobilized on the surface of the gold film. The arising mass loading causes a phase shift in the electric signal to be measured by an electronic circuit.

One can impress the aptamer layer as a periodic bristle structure on the top of the gold film contacting with the liquid (see Figure 1). The thickness of the aptamer layer is about 4 nm and the number of bristles per surface unit is enormous large. Therefore, the direct numerical modeling of such a structure using fluid-solid interface conditions is impossible. Proper models can be derived using the homogenization technique from [2] and [3] along with the strict treatment of the fluid-solid interface (see e.g. [4]).

A homogenization technique for the treatment of the bristle structure is proposed. The bristle-fluid structure is replaced by an averaged material whose properties are derived as the number of bristles goes to infinity whereas their thickness goes to zero. The fluid-solid interface conditions are accounted when passing to such a limit. The height of the bristles remains constant.

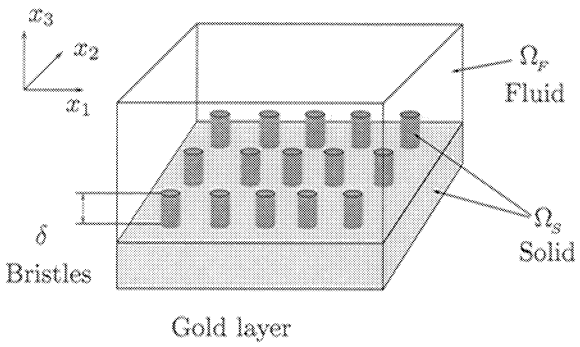

Figure 1: *Coupled system:* $\Omega = \Omega_F \cup \Gamma \cup \Omega_S$

The difference to known homogenized models like e.g. [5] proposed for the simulation of rigid rough surface-fluid interfaces consists in the assumption that the solid part is elastic. The fluid is assumed to be weakly compressible and the velocities in the fluid being sufficiently small. This enables the usage of the linearized Navie-Stokes equations. The motion of the solid is described by linear elasticity equations. On the fluid-solid interface, the continuity of normal pressures and velocities (no-slip condition) is assumed. The no-slip condition is the most hard to treat. We apply the approach proposed by J.-L. Lions in [6] which consists in the usage of the velocity instead of the displacement as the state variable for the solid. Using two-scale convergence, we obtain a limiting equation that describes a new material possessing some interesting properties: 1) the elastic modules decrease comparing to the ones of the bristle material but some resistance force which is proportional to the strain velocity appears; 2) the shear elastic modules vanish; 3) some short memory with respect to the strain arises. Thus, we obtain a thin layer made of a new material which contact the liquid from above and the solid body from below.

Using the model of the new material, we compute a

dispersal relation which expresses the dependence of the surface shear wave velocity on the excitation frequency. Based on the dispersal relation, one can compute many useful characteristics, for example, the sensitivity of the biosensor with respect to adhering ligand-biomolecules. Numerical algorithms developed by the authors work for any number of anisotropic layers. The precision of the method enables to estimate the sensitivity regarding nanoscopic mass loadings.

2 MATHEMATICAL MODEL

A coupled system modeling a periodic bristle or pin structure contacting with a fluid is shown in Figure 1. The solid part consists of a substrate and pins located on its top. The pin structure is assumed to be periodic in (x_1, x_2) and independent of x_3. The total domain of the coupled system is denoted by $\Omega \subset \mathbb{R}^3$. The domains occupied by the fluid and elastic continua are denoted by Ω_F and Ω_S, respectively; the boundary separating the continua is called Γ.

2.1 Equations for Fluid-solid Interface

The coupled system is described by the following equations

$$\rho_F \boldsymbol{u}_t = -\nabla p + \mathrm{div} P\boldsymbol{u}_{\boldsymbol{x}} + \rho_F \boldsymbol{f} \quad \text{in} \quad \Omega_F, \qquad (1)$$

$$\gamma p_t = -\mathrm{div}\boldsymbol{u} \quad \text{in} \quad \Omega_F, \qquad (2)$$

$$\rho_S \boldsymbol{v}_{tt} = \mathrm{div}\, G\boldsymbol{v}_{\boldsymbol{x}} + \rho_S \boldsymbol{f} \quad \text{in} \quad \Omega_S. \qquad (3)$$

The no-slip and pressure equilibrium conditions on the fluid-solid interface read

$$\boldsymbol{v}_t = \boldsymbol{u} \quad \text{on} \quad \Gamma, \qquad (4)$$

$$G\boldsymbol{v}_{\boldsymbol{x}} \cdot \boldsymbol{n} = \big(-pI + P\boldsymbol{u}_{\boldsymbol{x}} \big) \cdot \boldsymbol{n} \quad \text{on} \quad \Gamma, \qquad (5)$$

whereas the boundary and initial conditions are trivial for simplicity. Here, ρ_F and ρ_S are the densities of the fluid and the solid parts, respectively; $\boldsymbol{u}$ is the velocity field of the fluid, p is the pressure in the fluid, $\boldsymbol{v}$ is the displacement field of the solid part, $\boldsymbol{f}$ is an external force like the gravity. The coefficient γ characterizes the compressibility of the fluid. The fourth-rank tensors P and G are of the following form

$$P\boldsymbol{u}_{\boldsymbol{x}} = \lambda\, \mathrm{div}\boldsymbol{u}\, I + \mu\, D(\boldsymbol{u}), \quad G\boldsymbol{v}_{\boldsymbol{x}} = l_1\, \mathrm{div}\boldsymbol{v}\, I + l_2\, D(\boldsymbol{v}).$$

The second-rank unit tensor I has the components $I_{ij} = \delta_{ij}$, where δ_{ij} is the Kronecker symbol. The strain velocity tensor $D(\boldsymbol{u})$ has, as usually, the components $D_{ij}(\boldsymbol{u}) = 1/2\,(\partial u_i/\partial x_j + \partial u_j/\partial x_i)$. The symbols λ and μ denote positive balk and dynamic viscosity coefficients of the fluid, respectively; l_1 and l_2 are Lamé coefficients of the solid part if the solid phase is isotropic. As usually, the summation over repeating indices is assumed, $\boldsymbol{n}$ denotes the normal vector to a surfaces or curve. Note that the components of the elastic stiffness tensor G can be arbitrary up to base restrictions so that arbitrary *anisotropic solids* can be considered.

The no-slip condition (4) is the main handicap for the mathematical treatment of the model (1)-(5). The method from [6] is used to overcome this difficulty by utilizing the velocity instead of the displacement in equation (3). This is being done by introducing the following integral operator

$$\mathcal{J}_t \boldsymbol{w} = \int_0^t \boldsymbol{w}(s) ds.$$

Now, equation (3) can be rewritten in the form

$$\rho_S \boldsymbol{u}_t = \mathrm{div}\, G\mathcal{J}_t \boldsymbol{u}_{\boldsymbol{x}} + \rho_S \boldsymbol{f}, \qquad (6)$$

where $\boldsymbol{u} = \boldsymbol{v}_t$. The pressure p can be expressed through the velocity $\boldsymbol{u}$ from equation (3) as follows

$$p = -\gamma^{-1} \mathrm{div}\mathcal{J}_t \boldsymbol{u}. \qquad (7)$$

2.2 Refinement of the Pin Structure

A refinement parameter ε will be introduced so that the value $\varepsilon = 1$ corresponds to the original structure but the number of pins grows, and the pins become finer whenever $\varepsilon \to 0$. Let χ be the characteristic function of the domain Ω_F. This function will be redefined so that it becomes dependent on the refinement parameter. Assume that the (x_1, x_2)-projection of the base cell of the pin structure is a square and scale this square to the unit square $\Sigma = [0,1] \times [0,1]$. The (x_1, x_2)-projection of the solid part of the base cell will be transformed into a subset $\Sigma_S \subset \Sigma$. Denote the domain $\Sigma \setminus \overline{\Sigma}_S$ by Σ_F. The domain Σ is called structural cell (see Figure 2).

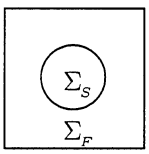

Figure 2: *Structural cell* $\Sigma = [0,1] \times [0,1]$

Let $\hat{\boldsymbol{x}} = (x_1, x_2)$ and $\hat{\chi}(\hat{\boldsymbol{x}})$ be the Σ-periodic extension of the characteristic function of the domain Σ_F to all $\mathbb{R}^2$. We define the modified function χ^ε as follows (remember that δ is the thickness of the pin layer):

$$\chi^\varepsilon(\boldsymbol{x}) = \begin{cases} 1, & x_3 > \delta, \\ \hat{\chi}(\dfrac{\hat{\boldsymbol{x}}}{\varepsilon}), & -\delta \leqslant x_3 \leqslant \delta, \\ 0, & x_3 < -\delta. \end{cases} \qquad (8)$$

Let us rewrite equations (1), (2), and (3) as one equation with discontinues coefficients in the whole domain

Ω using the introduced characteristic function χ^ε. The equation reads

$$\rho^\varepsilon \boldsymbol{u}_t^\varepsilon = \mathrm{div} \boldsymbol{M}^\varepsilon \boldsymbol{u}_{\boldsymbol{x}}^\varepsilon + \rho^\varepsilon \boldsymbol{f}, \tag{9}$$

where

$$\rho^\varepsilon = \rho_F \chi^\varepsilon + \rho_S (1 - \chi^\varepsilon),$$
$$\boldsymbol{M}^\varepsilon = \chi^\varepsilon P + \left(\chi^\varepsilon \gamma^{-1} I \otimes I + (1 - \chi^\varepsilon) G\right) \mathcal{J}_t.$$

The interface condition (4) is equivalent to the continuity of $\boldsymbol{u}^\varepsilon$ on Γ but the condition (5) assumes now the form

$$G \mathcal{J}_t \boldsymbol{u}_{\boldsymbol{x}}^\varepsilon \cdot \boldsymbol{n} = \left(\gamma^{-1} \mathrm{div} \mathcal{J}_t \boldsymbol{u}^\varepsilon \cdot I + P \boldsymbol{u}_{\boldsymbol{x}}^\varepsilon\right) \cdot \boldsymbol{n} \quad \text{on } \Gamma^\varepsilon, \tag{10}$$

when accounting (7).

Theorem 2.1 *If $\boldsymbol{f}, \boldsymbol{f}_t \in L^2([0,T] \times \Omega)$, then a unique weak solution to problem (9), (10) satisfies the estimate*

$$\mathrm{ess\,sup}_{t \in (0,T)} \left(\|\boldsymbol{u}_t^\varepsilon(t)\|_{L^2(\Omega)} + \|\boldsymbol{u}_{\boldsymbol{x}}^\varepsilon(t)\|_{L^2(\Omega)}\right) \leqslant C, \tag{11}$$

where C is an independent of ε constant.

Theorem 2.1 ensures the existence of subsequences $\{\boldsymbol{u}^{\varepsilon_k}\}$ that converge to limiting functions $\boldsymbol{u}$. Using a two-scale convergence technique by G. Nguetseng and G. Allaire (see [7], [8], and [9]), one can show that all limiting functions satisfy the same limiting equation. From the uniqueness of solutions of the limiting equation, one concludes that the sequence $\boldsymbol{u}^\varepsilon$ itself converges to an unique limiting function $\boldsymbol{u}$.

2.3 Limiting Equations

The two scale technique enables to derive the limiting equations. Nevertheless, the determination of their structure and computation of their coefficients is a challenge. Let Ω be divided into three parts

$$\Omega^f = \{\boldsymbol{x} \in \Omega \,|\, x_3 > \delta\},$$
$$\Omega^s = \{\boldsymbol{x} \in \Omega \,|\, x_3 < -\delta\},$$
$$\Omega^h = \{\boldsymbol{x} \in \Omega \,|\, \delta < x_3 < -\delta\}.$$

The limiting equations corresponding to the problem (9),(10) are of the form

$$\Omega^f: \ \rho_F \boldsymbol{u}_t - \mathrm{div}\, P \boldsymbol{u}_{\boldsymbol{x}} - \gamma^{-1} \nabla \mathrm{div}\, \mathcal{J}_t \boldsymbol{u} = \rho_F \boldsymbol{f}, \tag{12}$$
$$\Omega^s: \ \rho_S \boldsymbol{u}_t - \mathrm{div}\, \mathcal{J}_t G \boldsymbol{u}_{\boldsymbol{x}} = \rho_S \boldsymbol{f}, \tag{13}$$
$$\Omega^h: \ \rho_\theta \boldsymbol{u}_t - \mathrm{div}\, \overline{P} \boldsymbol{u}_{\boldsymbol{x}} - \mathrm{div} \mathcal{J}_t \overline{G} \boldsymbol{u}_{\boldsymbol{x}} - \mathrm{div} \int_0^t \omega(t-s) \boldsymbol{u}_{\boldsymbol{x}}(s)\, ds = \rho_\theta \boldsymbol{f}. \tag{14}$$

The physical conditions on the interfaces between Ω^h and Ω^f and between Ω^h and Ω^s are being derived from a weak formulation which precedes and yields equations (12)–(14). Note, that equations (12) and (13) coincide with (1) and (6), respectively. Thus, the governing equations for the pure fractions remain unchanged by the homogenization, which has been of course expected. What we have new, is integral-differential equation (14) which can not be reduced to a pure differential equation by differentiating or by a substitution like $\boldsymbol{w} = \mathcal{J}_t \boldsymbol{u}$. The computation of the tensors $\overline{P}$, $\overline{G}$, and $\omega(\tau)$ is based on an analytical representation of solutions of the so-called cell equation which arises in homogenization theory. The difficulty is that the cell equation is not resolved with respect to the time derivative of the unknown function in our case. This handicap is overcome by restricting the cell equation to a certain subspace providing invertibility of the involved operators.

The computation of the tensors $\overline{P}$, $\overline{G}$, and $\omega(\tau)$ is being done with finite elements. The next theorem states their properties which provide the well-posedeness of equation (14).

Theorem 2.2 *There exists a positive constant C such that*

$$\overline{P}_{ijkl} \mathcal{Z}_{ij} \mathcal{Z}_{kl} \geqslant C\, |\mathcal{Z}|^2, \quad \overline{G}_{ijkl} \mathcal{Z}_{ij} \mathcal{Z}_{kl} \geqslant 0$$

for every second-rank tensor $\mathcal{Z}$, where $|\mathcal{Z}|^2 = \mathcal{Z}_{ij} \mathcal{Z}_{ij}$. The tensor $\overline{G}$ is degenerated, and $\overline{G}_{ijkl} \mathcal{Z}_{ij} \mathcal{Z}_{kl} = 0$ if and only if $\mathcal{Z}_{11} + \mathcal{Z}_{22} = 0$ and $\mathcal{Z}_{33} = 0$.

As one can see from equation (14), the tensor $\overline{G}$ is the elastic stiffness tensor for the homogenized continuum. Theorem 2.2 says that the homogenized material has rather new properties. Namely, it does not resist to the deformation, if the first invariant and the component (3,3) of the corresponding strain tensor are equal to zero. In other words, such deformations do not produce any stresses. Such a class of deformations is sufficiently large: it contains all deformations which do not change the volume. Note that the tensor $\omega(\tau)$ falls very rapidly, if τ grows. The time scale is about 10^{-11}s for typical material parameters.

3 SIMULATION RESULTS

Using the derived model, we simulate a Love wave sensor based on the multi-layered structure shown in Figure 3. The molecular layer adhering to the surface of the auxiliary gold layer is being modeled through the homogenization technique developed in this paper. The molecular layer is expected being well described as a new material associated with equation (14). Equations (12) and (13) describe then the overlaying fluid and the underlying gold layer. Such a model allows us to compute the dispersal relation which expresses the dependence of the velocity of surface shear waves on the excitation frequency. The sensitivity is being computed as $(\bar{\omega}_R - \omega_R)/\Delta m$ where $\bar{\omega}_R$ and ω_R are the resonance frequencies for the loaded and unloaded sensor,

respectively. The resonance frequency is defined from the equation $\lambda(\omega_R) = 40\mu m$. Here λ is the wave length and $40\mu m$ is the period of the input IDTs.

Figure 4 presents computed graphs of the sensitivity versus the guiding layer thickness for the Love wave sensor. The loading is modeled through doubling the thickness of the homogenized layer. The thickness of the gold layer is being varied from 0.5 nm to 300 nm. The best sensitivity is achieved at 200 nm. Above this value, decreasing the sensitivity is observed. The light curve in Figure 4 corresponds to 300 nm thickness of the gold layer. The computation results are in a good agreement with physical experiments described in [10].

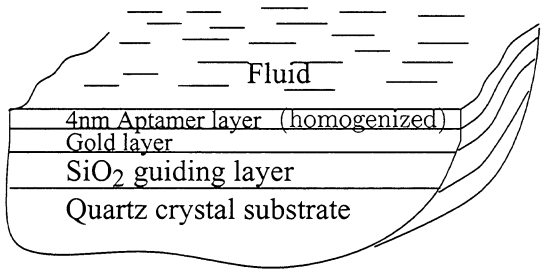

Figure 3: Multi-layered structure

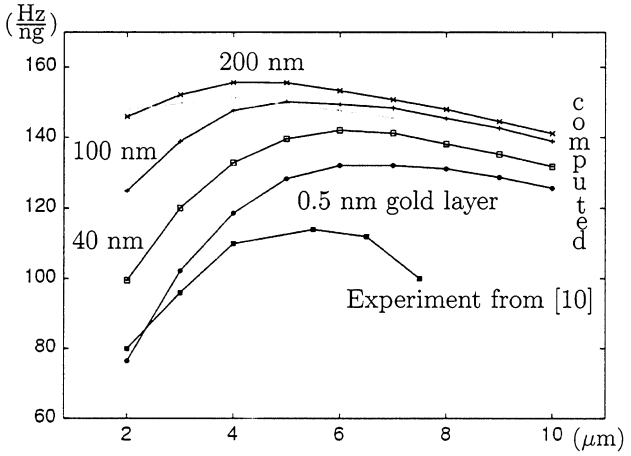

Figure 4: Comparison of numerically computed and experimentally measured sensitivities

The next simulation shows the sensitivity of the Love wave sensor regarding an additional homogenized protein layer which is being adhered to the aptamer layer (compare with Figure 3). The dependence on the aptamer packing density is presented. Thereby, the protein packing density is changing so that their ratio remains constant. The packing density is defined as $|\Sigma_S|/(|\Sigma_S| + |\Sigma_F|)$, see Figure 2. The thicknesses of the aptamer and protein layers are 21A and 43A, respectively.

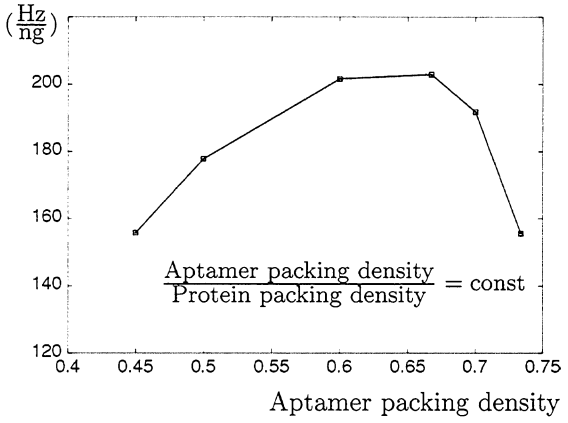

Figure 5: Sensitivity for various packing densities

REFERENCES

[1] N. Botkin, M. Schlensog, M. Tewes, and V. Turova, "A mathematical model of a biosensor", In: Technical Proceedings of the Fourth International Conference on Modeling and Simulation of Microsystems, Hilton Head Island, South Caroline, USA, 231–234, 2001.

[2] U. Hornung, "Homogenization and porous media", Springer, New York, 1997.

[3] K.-H. Hoffmann and N.D. Botkin, "Homogenization of von Kármán plates excited by piezoelectric patches", ZAMM **80**(9), 579–590, 2000.

[4] K.-H. Hoffmann and V.N. Starovoitov, "On a motion of a solid body in a viscous fluid. Two-Dimensional Case", Adv. Math. Sci. Appl. **9**(2), 633–648, 1999.

[5] W. Jäger and A. Micelić, "On the Roughness-Induced Effective Boundary Conditions for an Incompressible Viscous Flow", J. of Differential Equations **170**, 96–122, 2001.

[6] J.L. Lions, "Quelques méthodes de résolution des problèmes aux limites non linéaires", Dunod Gauthier-Villars, Paris, 1969.

[7] G. Nguetseng, "A general convergence result for a functional related to the theory of homogenization", SIAM J. Math. Anal. **20**(3), 608–623, 1989.

[8] G. Allaire, "Homogenization and two-scale convergence", SIAM J. Math. Anal **23**(6), 1482–1518, 1992.

[9] D. Lukkassen, G. Nguetseng, and P. Wall, "Two–scale convergence", International Journal of Pure and Applied Mathematics **2**(1), 35–86, 2002.

[10] G.L. Harding, "Mass sensitivity of Love-mode acoustic sensors incorporating silicon dioxide and silicon-oxy-fluoride guiding layers", Sensors and Actuators **A 88**, 20–28, 2001.